Fox and Li Approach

$$u_p = \frac{ik}{4\pi} \iint_A u_{p-1} \frac{\exp(-ikR)}{R} (1 + \cos(\theta)) dA$$

u_p — Electric field at the p-th iteration.

k — propagation constant

R — Distance from the observation
point to the source point

θ — Angle of R with respect to the
normalof the observation point.

Scalar Huygen's integral.

**Successively applied spatial filtering until
a steady state "mode" is established.**

oscillations is a result of attenuation of modes with higher losses. For these two
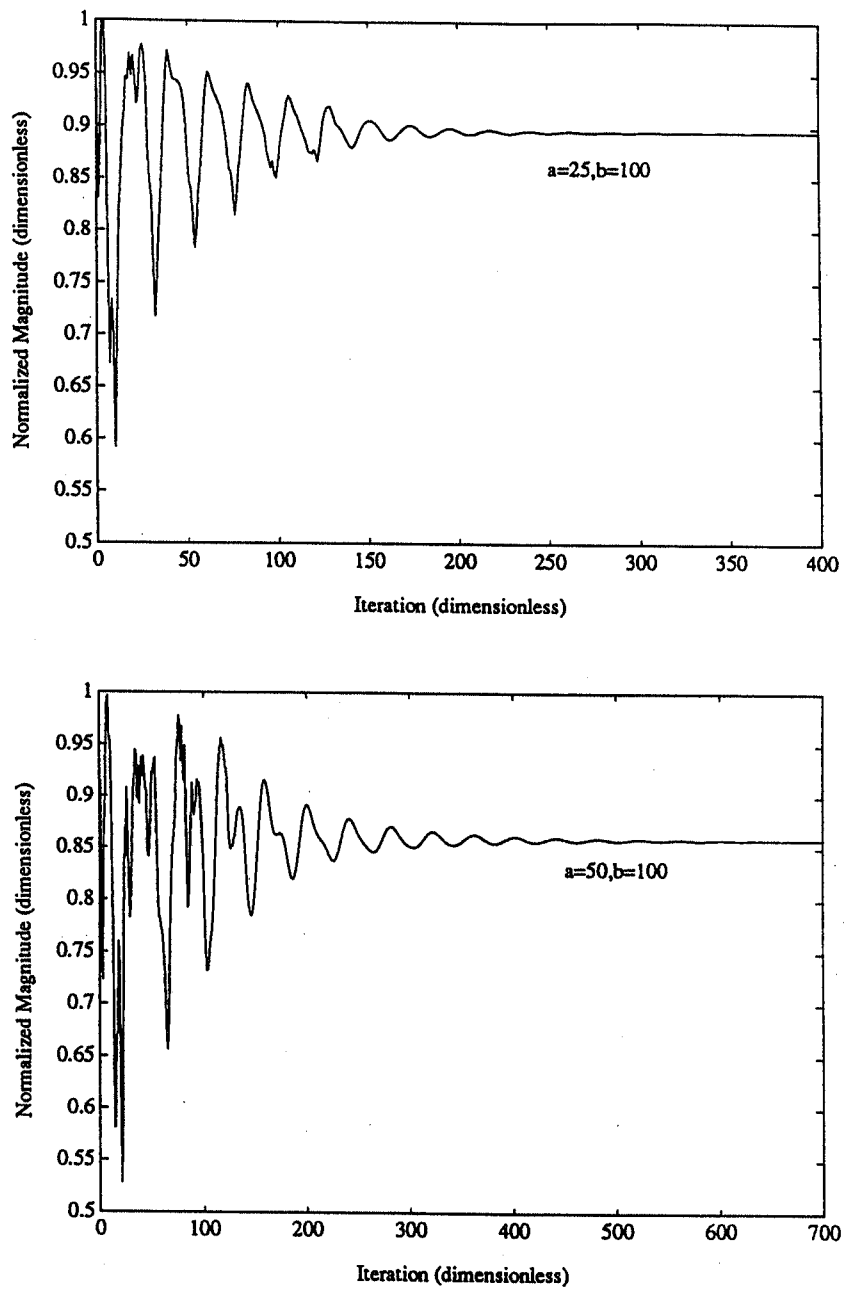

Figure A.1 mode settling in two cavities : Top a = 25 λ, b = 100 λ; Bottom a = 50 λ, b = 200 λ. The larger cavity takes twice as long to settle.
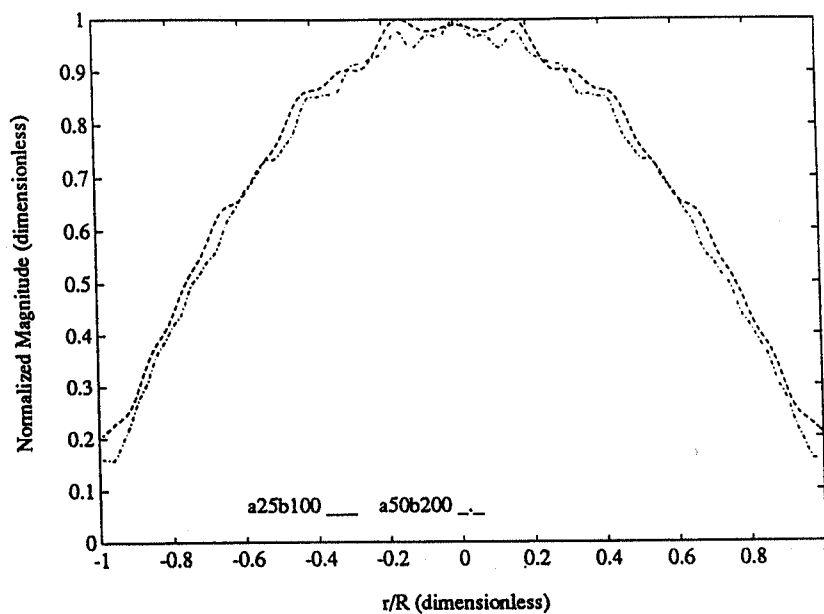
Figure A.2 Steady state normalized magnitudes for two cavities
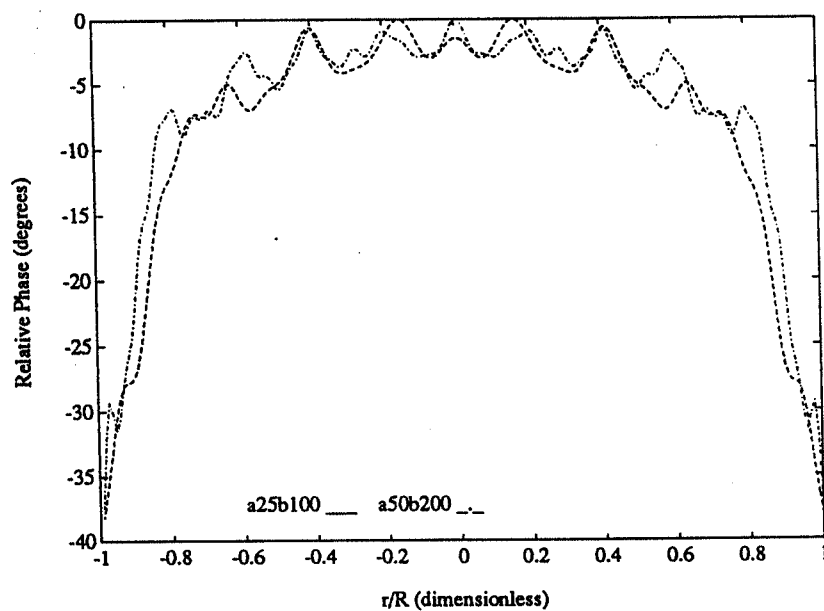twice as large as the other. The modes are very similar.

Figure A.3 Steady state relative phase profiles for two cavities
twice as large as the other. The modes are very similar.

cavities with same physical proportions, the similarity in the corresponding steady state magnitude and phase distributions is shown in Figs. A.2 and A.3. Keeping the length of our cavity 100λ, we vary the width of the cavity and observe an expected decrease in the mode settling (Fox-Li) number. As the cavity is made narrower, there is increased leakage and loss from the sides. This causes the lowest loss mode to dominate more quickly, and we see smaller mode settling numbers in Figure A4. For final magnitude distributions shown in Figure A.5,
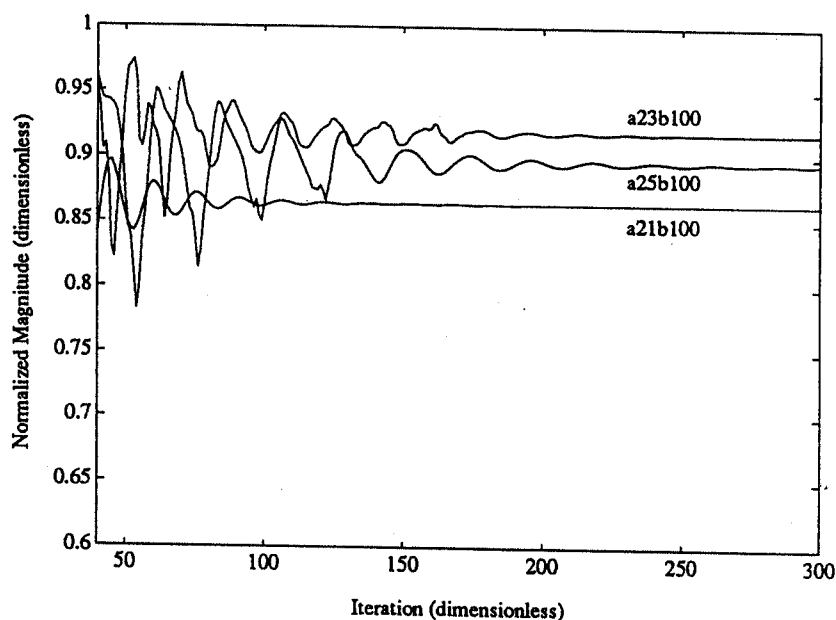

Figure A.4 mode settling plots for cavities of half widths a = 25 λ, a = 23 λ, a = 21 λ, and length b= 100 λ. We see decrease in the mode settling time as the width decreases.

the magnitude at the edges of the cavity is greater for narrower cavities. This

implies greater loss per pass through the amplifier. We plot the dependance of
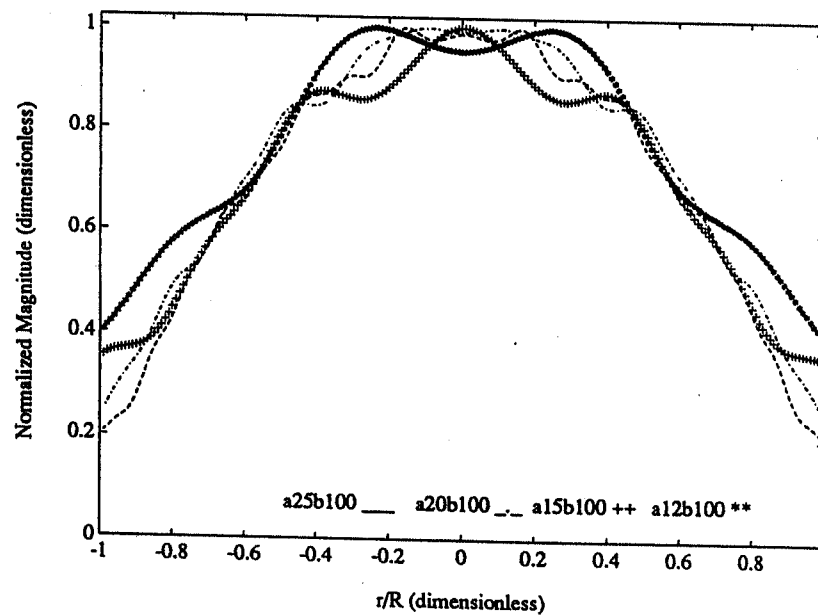

Figure A.5 Steady state normalized magnitude plots for cavities of half widths a = 25 λ, a = 23 λ, a = 21 λ, and length b= 100 λ. As the cavity is made narrower, the amplitude at the edge of the cavity is higher, implying greater loss per roundtrip.

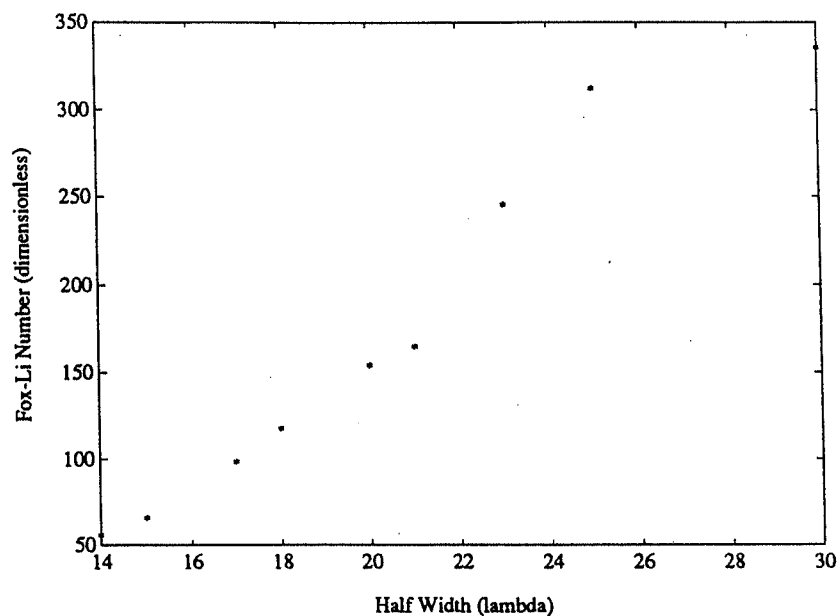the Fox-Li number on the width of the cavity in Figure A.6.

Figure A.6 Summary plot of fxli numbers as a function of the width of the cacity

We also calculate the time scale relevant to the system. We know that $time = \frac{distance}{speed}$ and $c = \frac{\lambda}{\nu}$, where c is the speed of light, λ is the wavelength and ν is the frequncy of the light. The length of the cavity is 100 λ. The time to traverse the cavity once is given by

$$t = \frac{100\,\lambda}{c}\; secs$$
$$= \frac{100}{\nu}\; secs$$

(A.2.1)

For blue light, ν is about 7.5×10^{14} Hz. For such a system the time to traverse is about 130 femtoseconds.
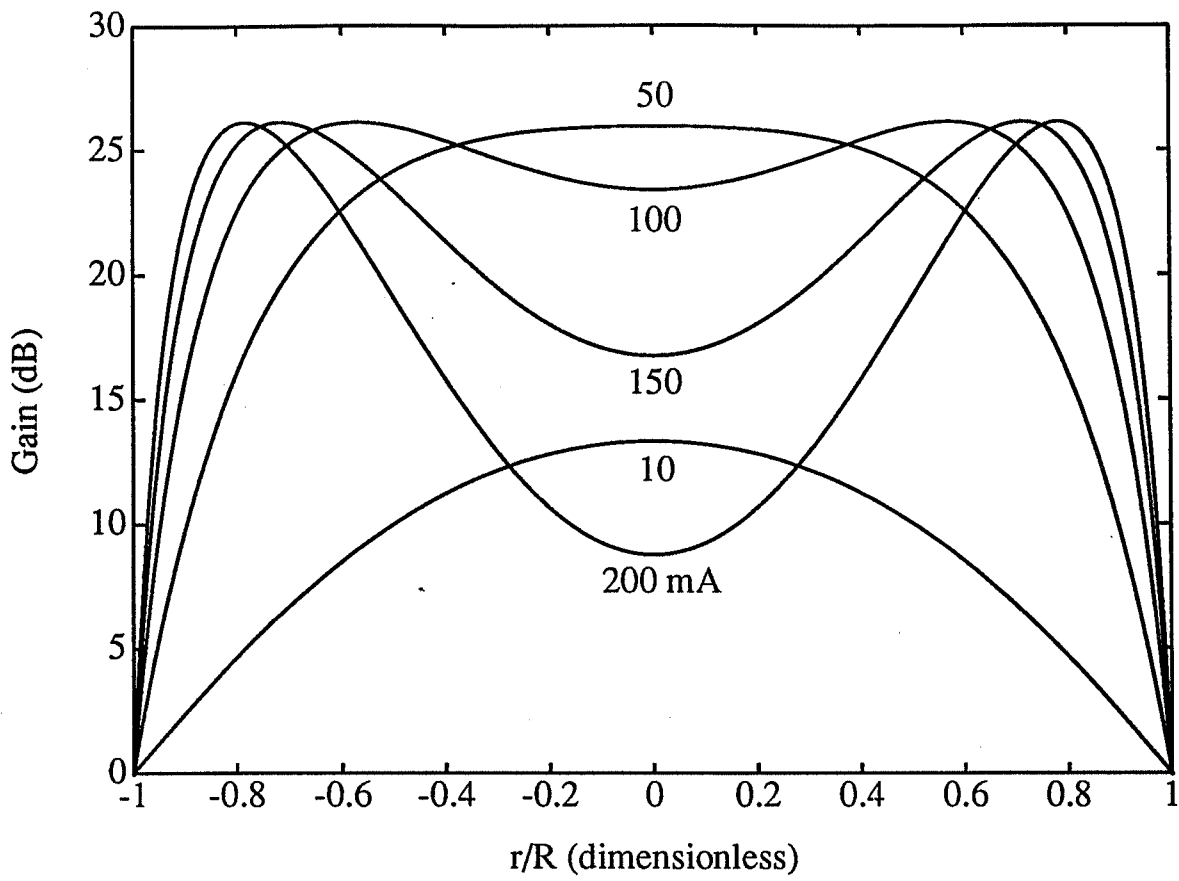
$$g(r) = \frac{\alpha\, i_d\, J_0\left(2.405\, s\, \frac{r}{R}\right)}{1 + b\, i_d\, J_0\left(2.405\, \frac{r}{R}\right)} - \beta\, i_d\, J_0\left(2.405\, \frac{r}{R}\right)$$
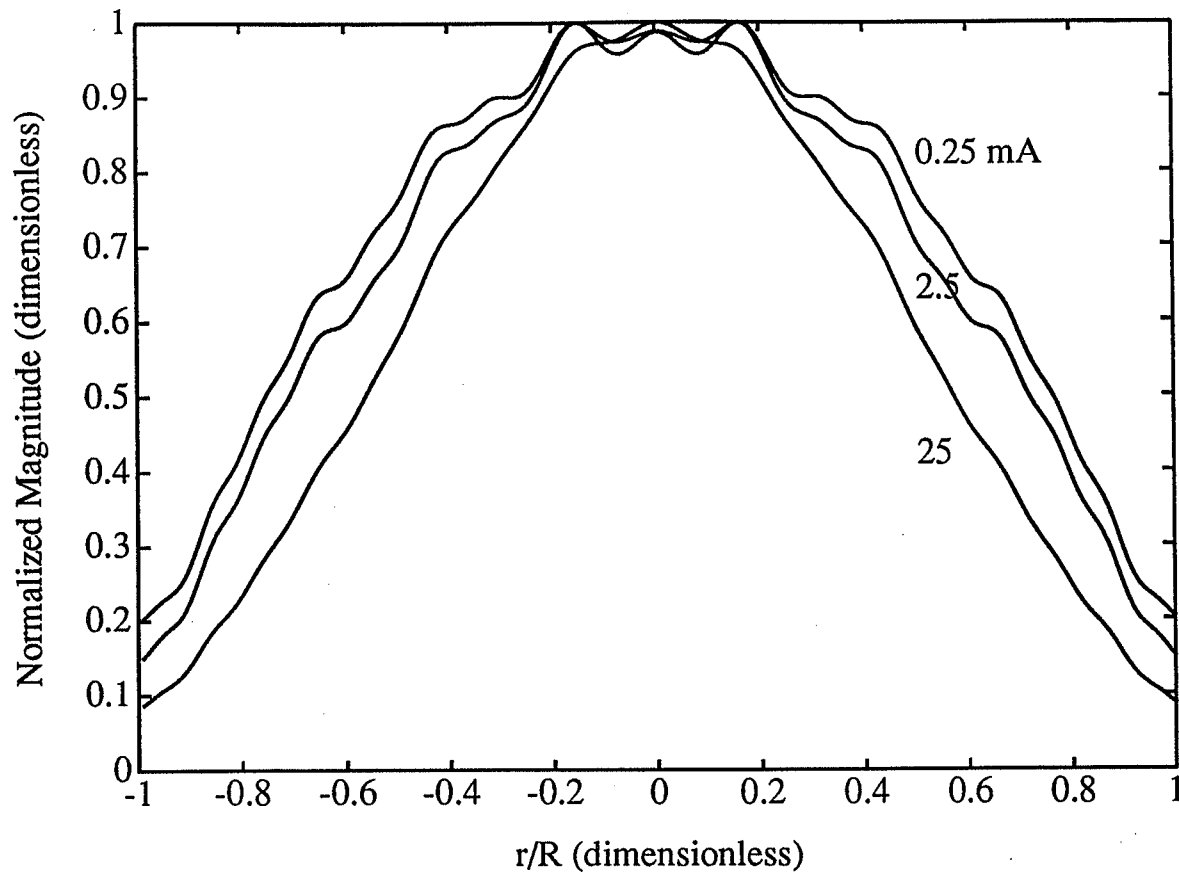
Fig. 1

Figure 2. Steady state modes for several low current values. In Fig. 2a are the amplitudes which correspond to i_d = 0.25, 2.5 and 25 mA. As the current increases the mode width decreases. The corresponding plots of the phase are shown in Fig. 2b. In Fig. 2c are the amplitudes which correspond to i_d = 25 mA, 50 mA and 82 mA. As the current continues to increase, the mode width starts to increase. The corresponding plots of the phase are shown in Fig. 2d.
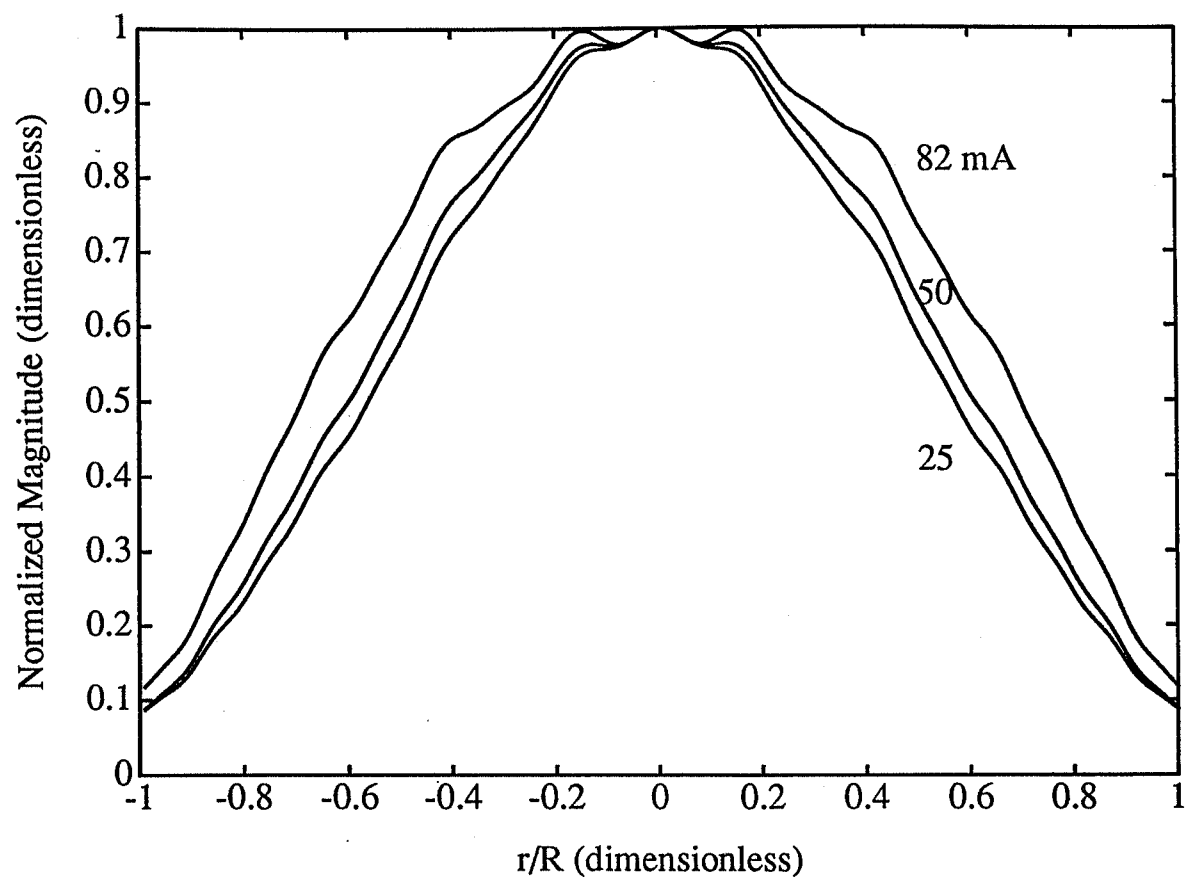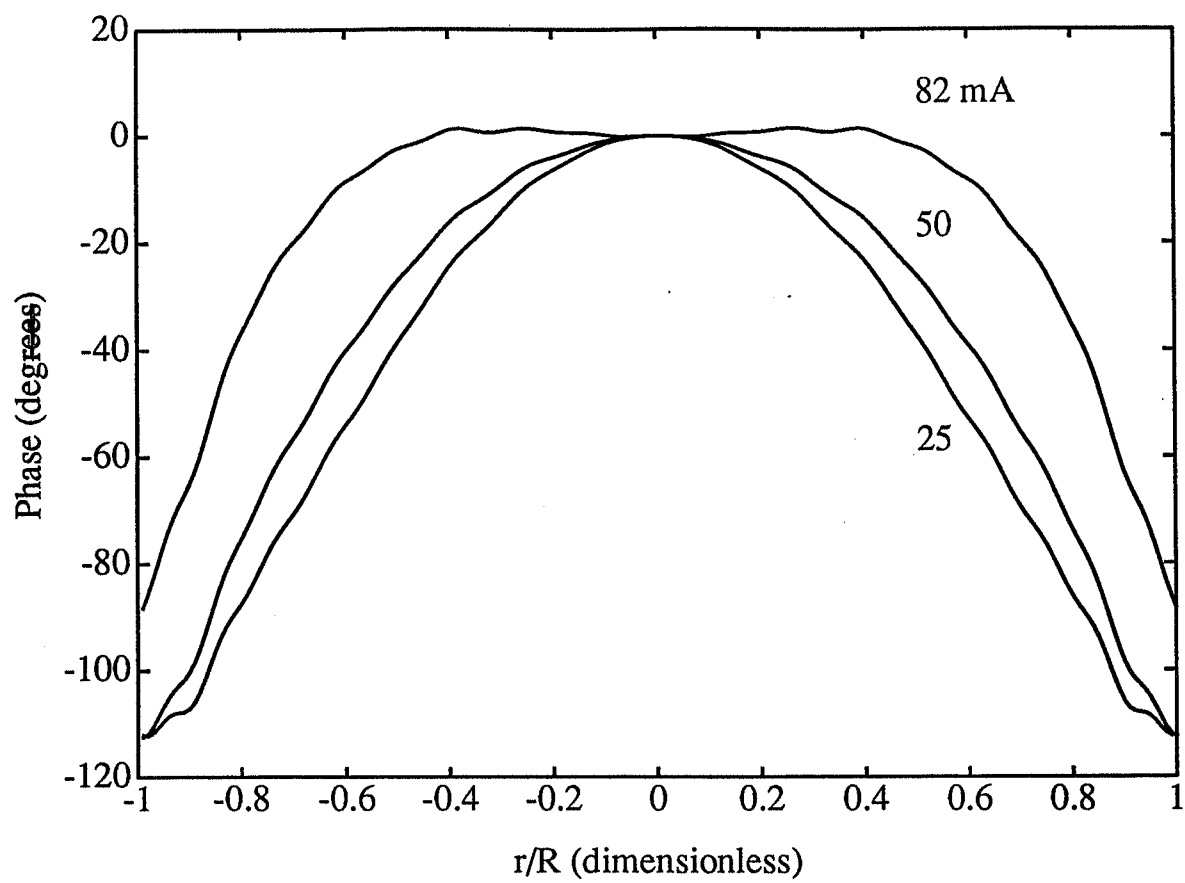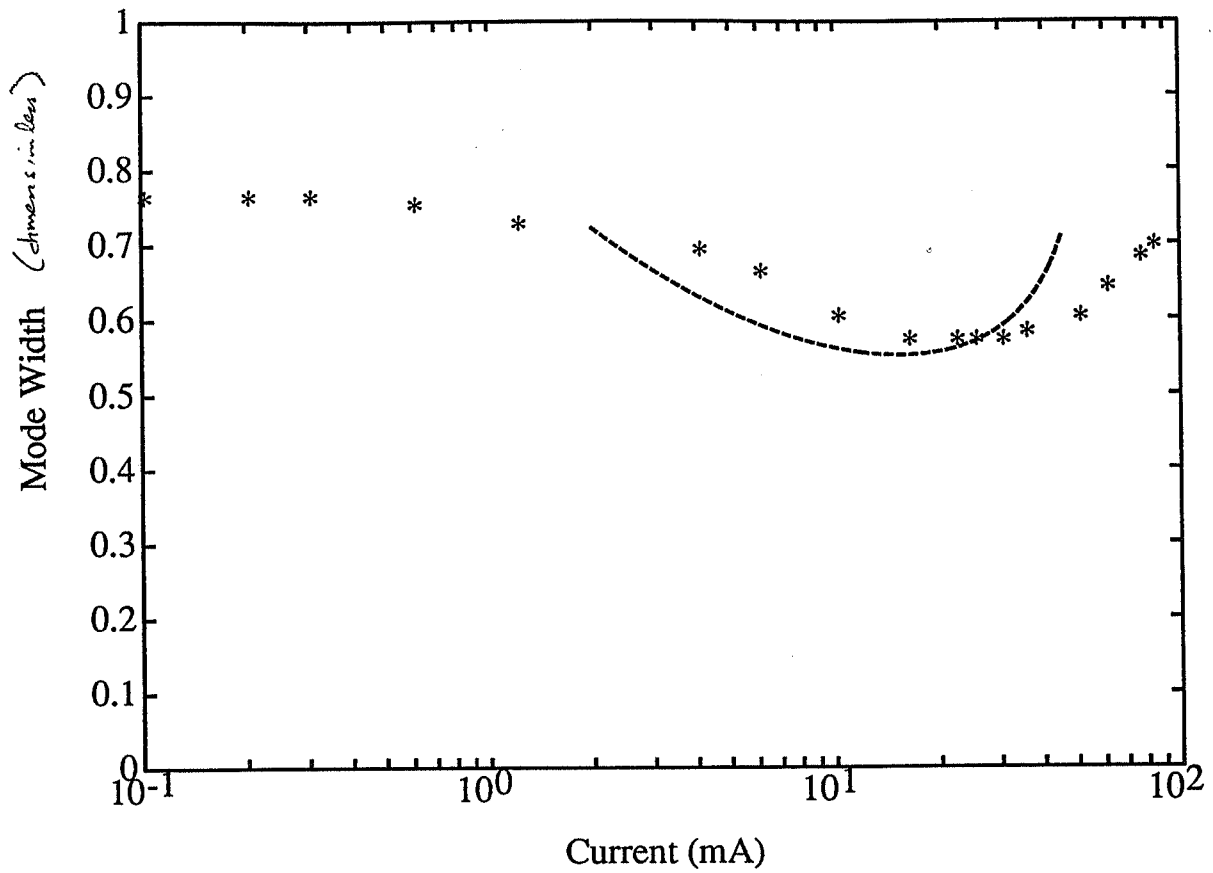
2 (a)

Fig. 2b
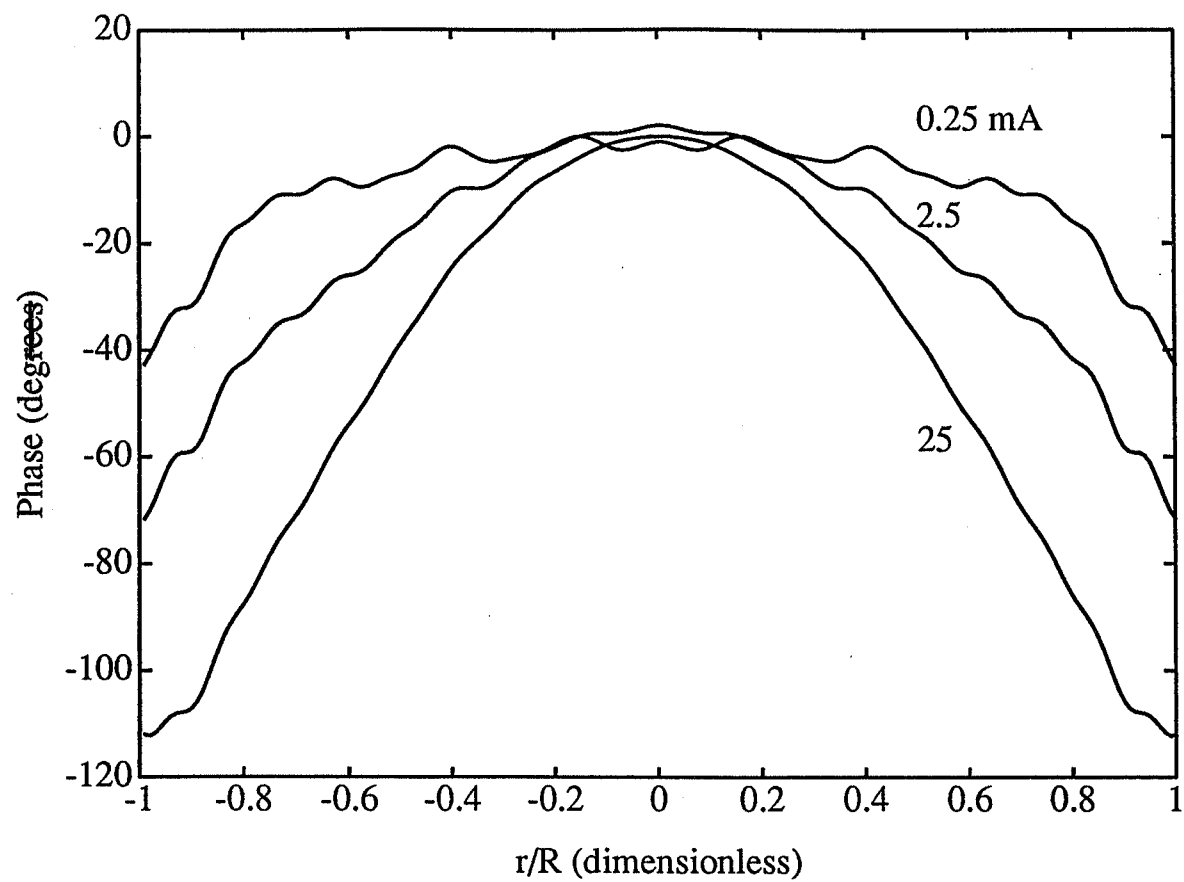
Fig. 2c

Fig. 2d

Figure 3. The full widths at half maximum, in units normalized to the cavity radius, of the Fox and Li steady state mode, w_{FL}, as a function of current are marked by the *'s. The dashed line is the curve of w_K calculated by Gaussian beam theory in a resonator with a quadratic gain medium.
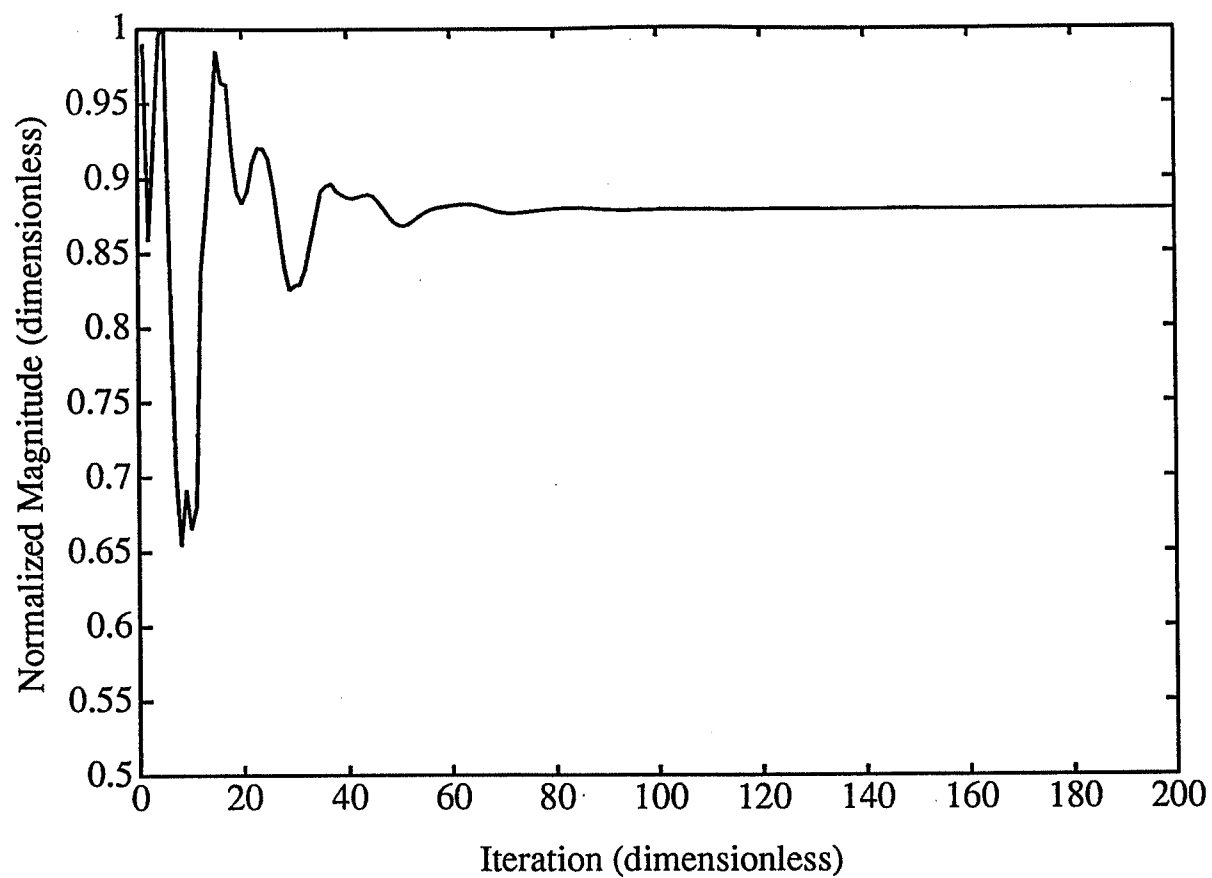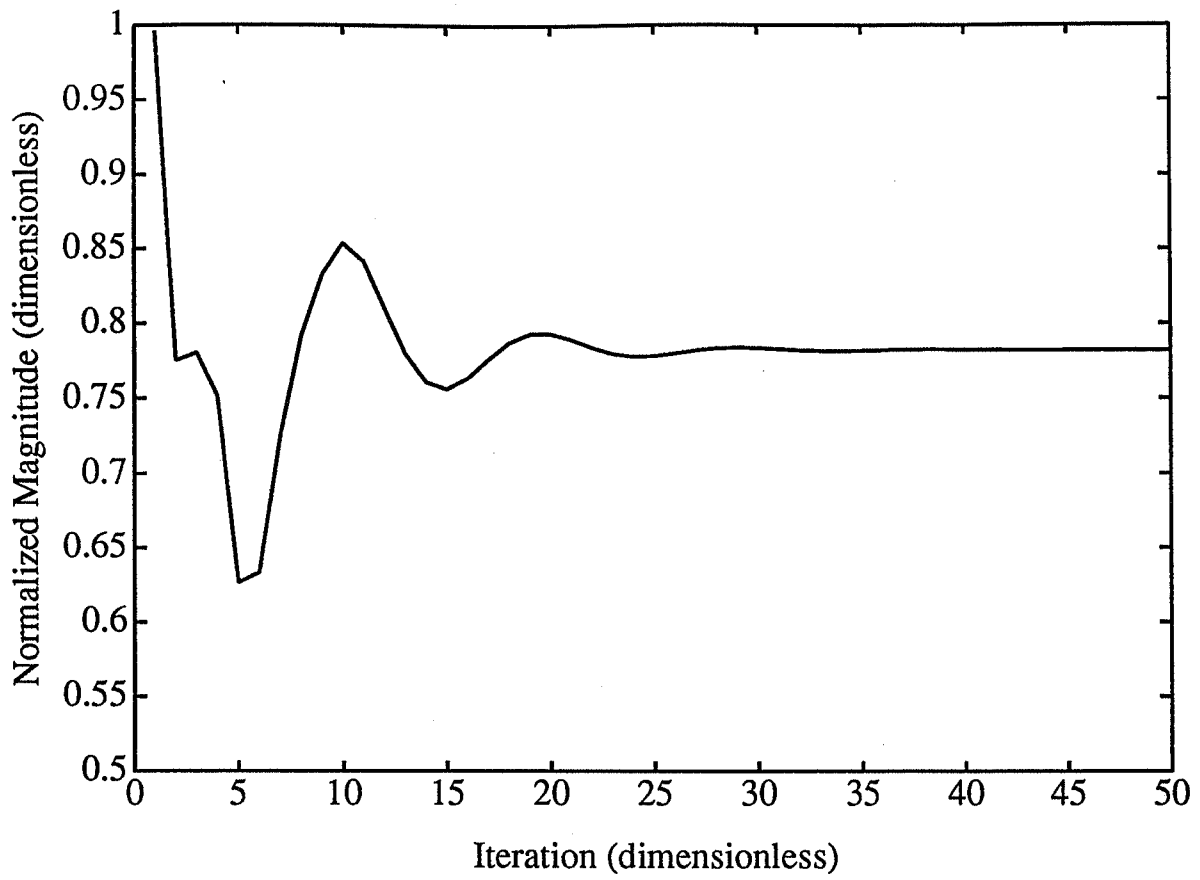
Fig. 3.

Figure 4. Fox and Li plots of the mode evolution over iterations of Eq. 1 calculated at several different currents: $i_d = 1$ mA in Fig 4a, 25 mA in 4b and 82 mA in 4c.
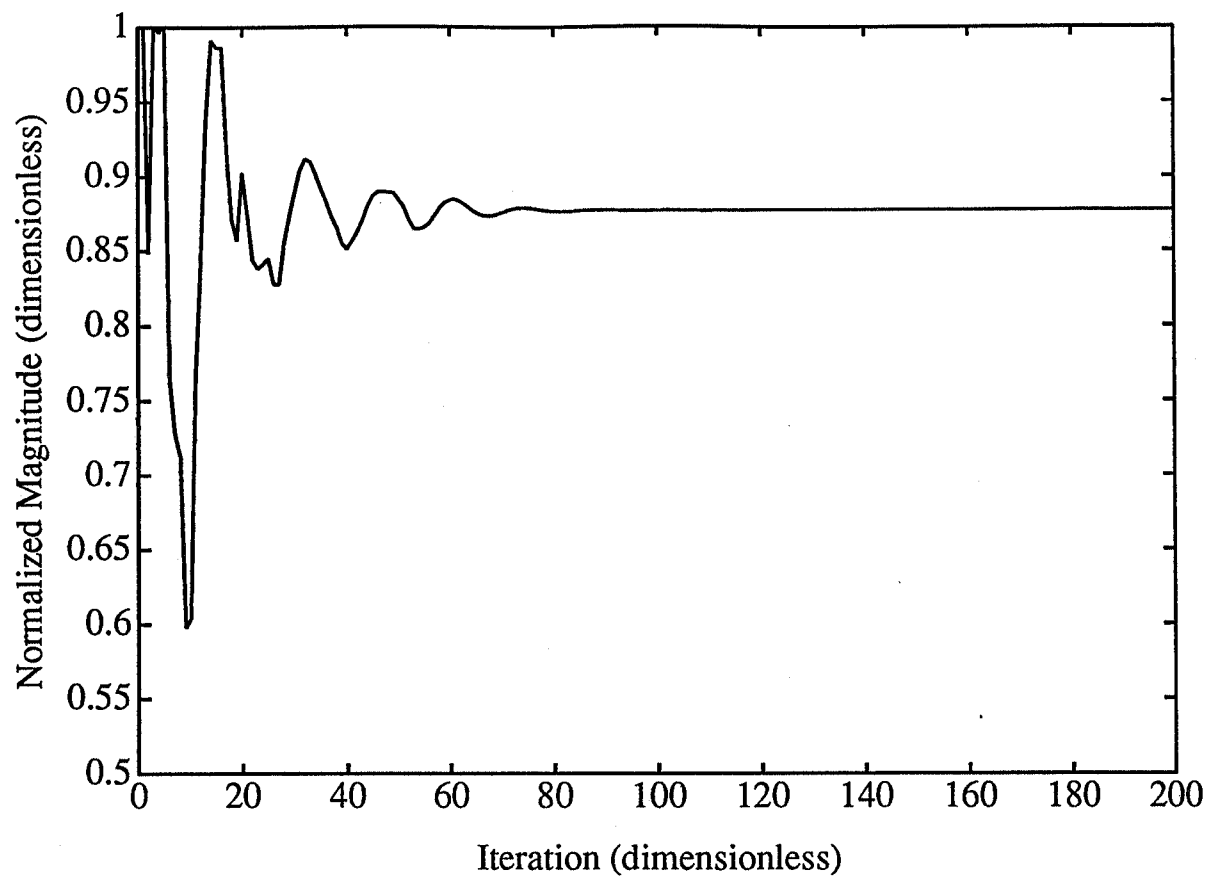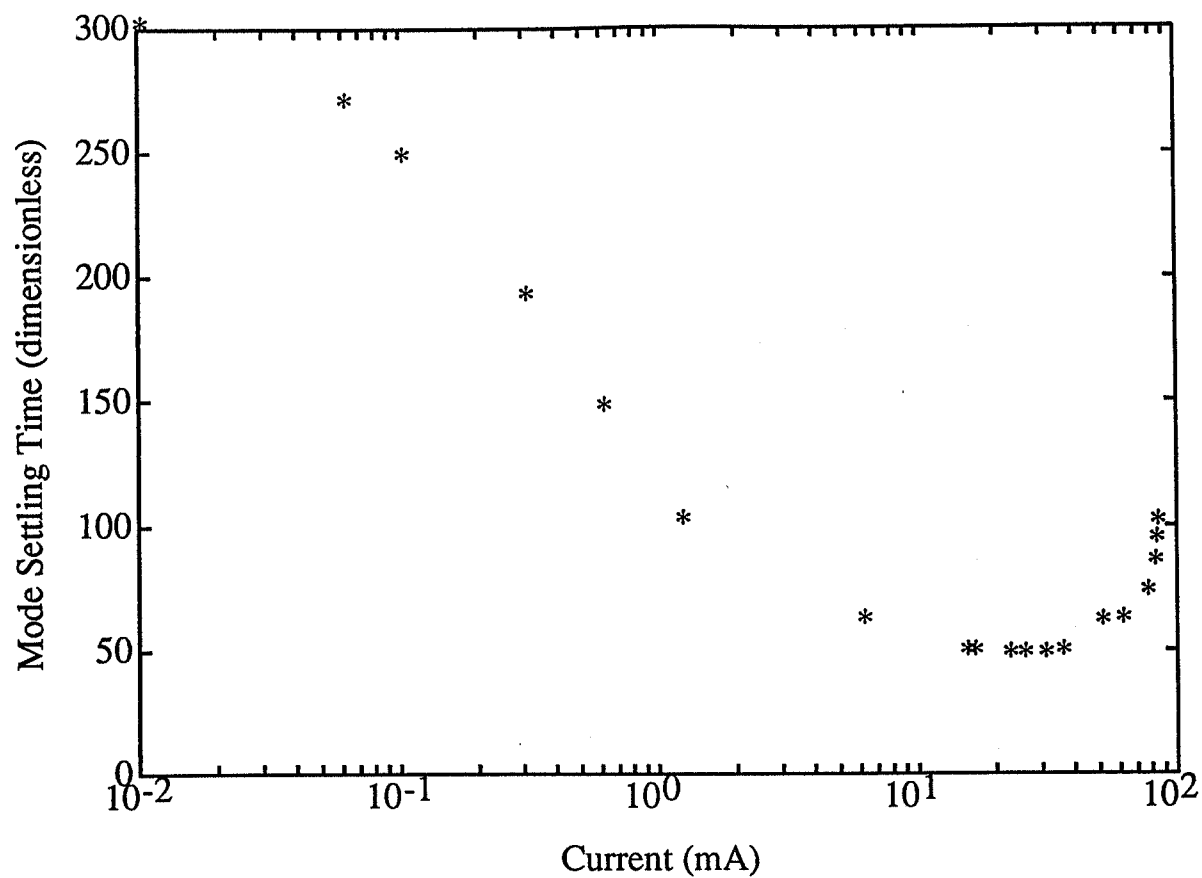
4 (a)

4(b)

Fig. 4b

4(c)

Fig. 4c

Figure 5. The mode settling time, or Fox and Li number, is plotted as a func[...] i_d. The shape of this curve is similar to the Fox and Li results plotted in Fig. ?[...]
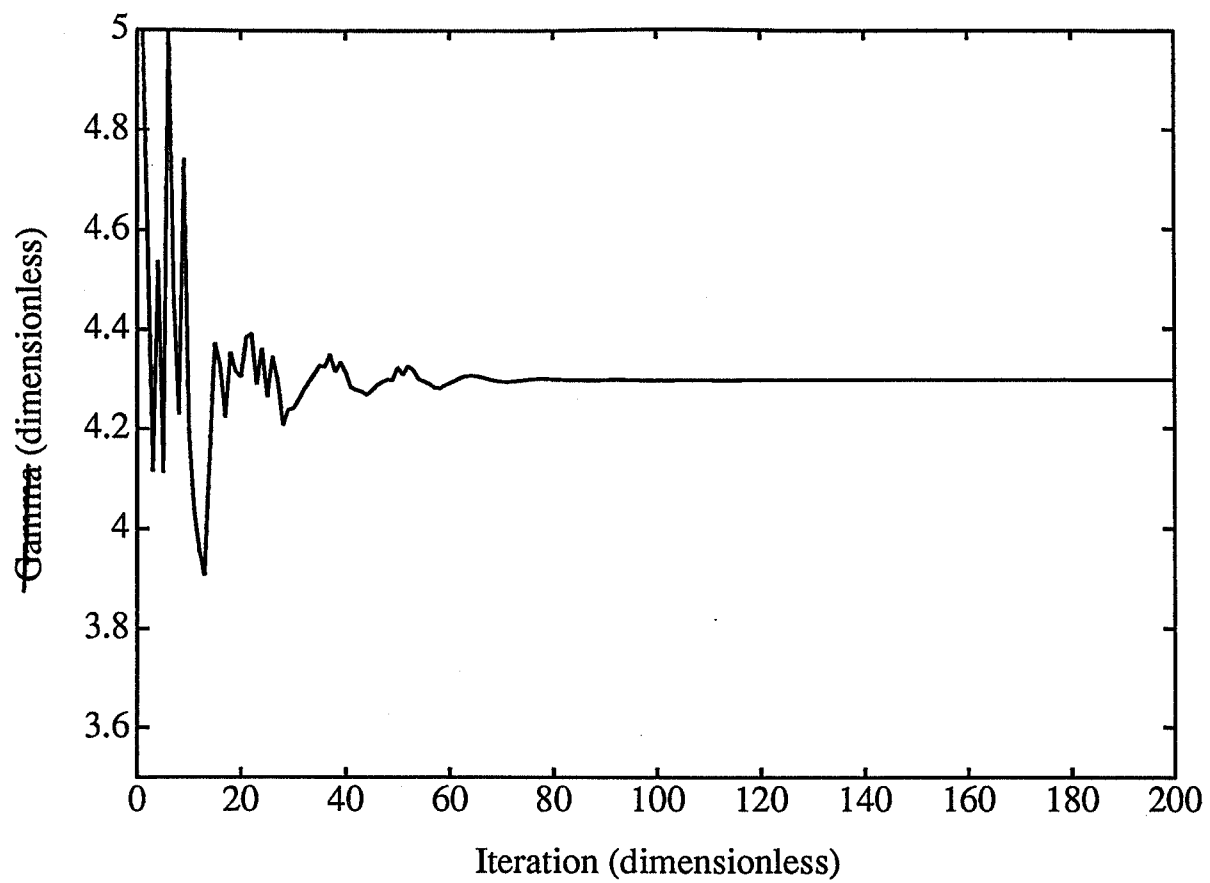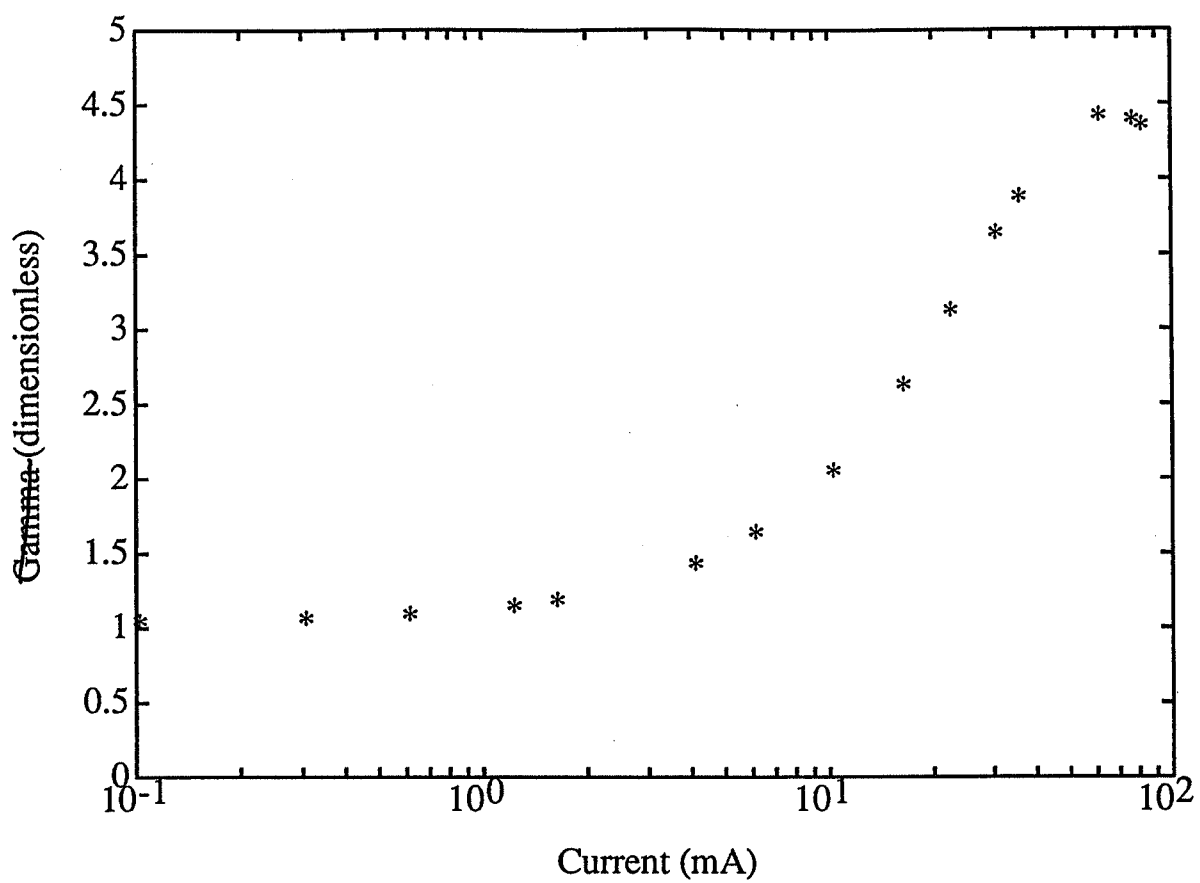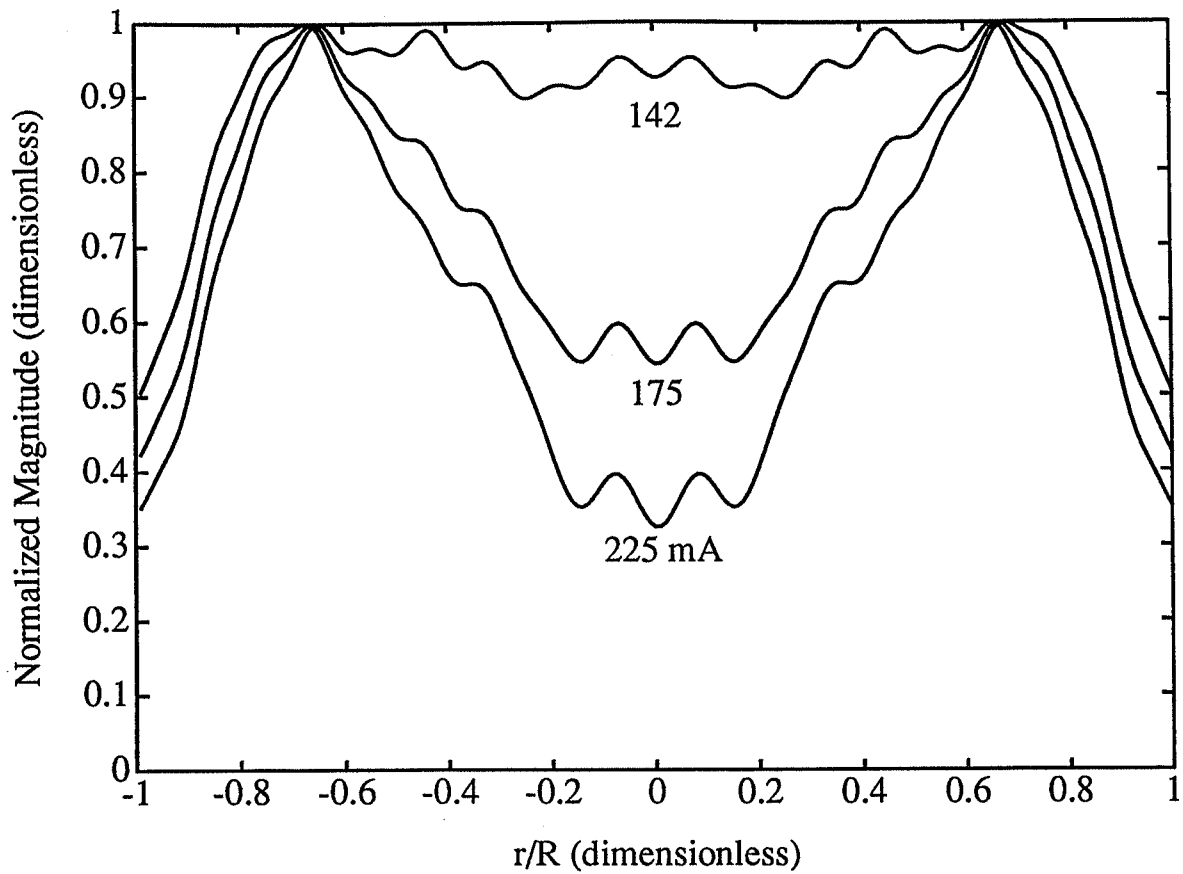
Fig. 5

Fig. 6

Fig. 7

Figure 8. Steady state modes for several high current values. The magnitudes for i_d = 142 mA, 175 mA and 225 mA are shown. As the current increases the gain becomes strongly annular, the steady state flat-topped beam of 142 mA may be of practical use in certain applications. The mode magnitudes are plotted in Fig. 8a. The relative phase distributions are plotted in Fig. 8b.
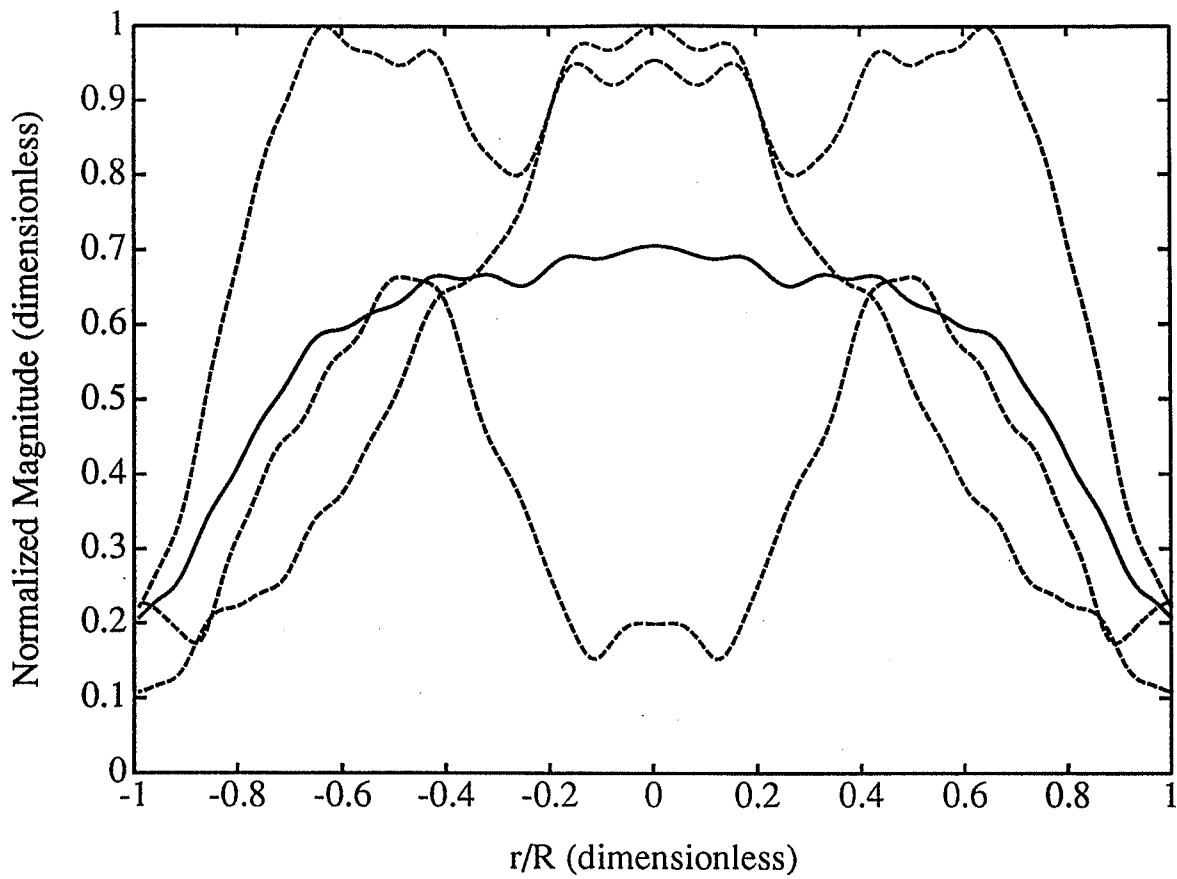
8 (a)

Fig. 8a
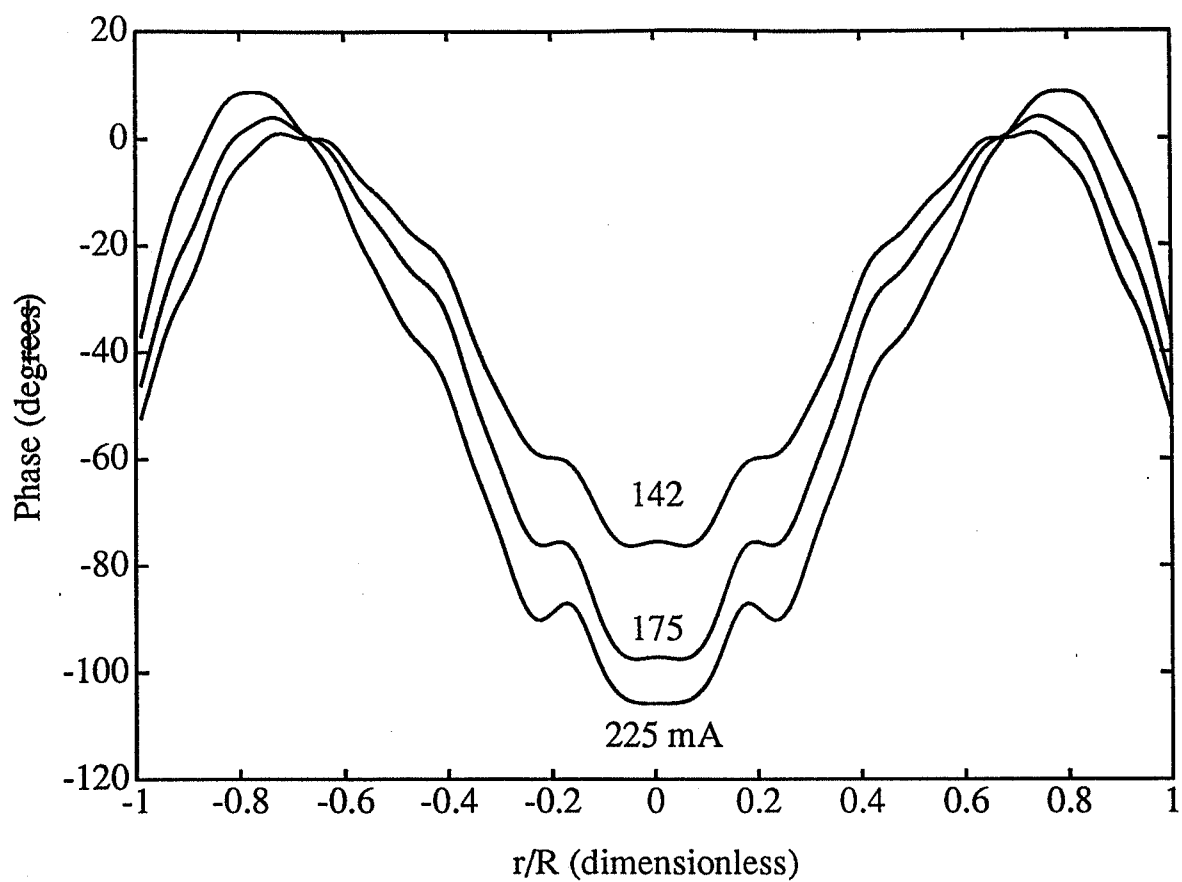
Fig. 8b

Figure 9. Field distribution magnitudes for $i_d = 100$ mA in the intermediate current regime. At this current value, the field oscillates through 21 states. Samples of the three dominant shapes — annular, tightly focussed, and flat-topped — are shown in dashed lines. The average of all 21 distributions in shown as a solid line.
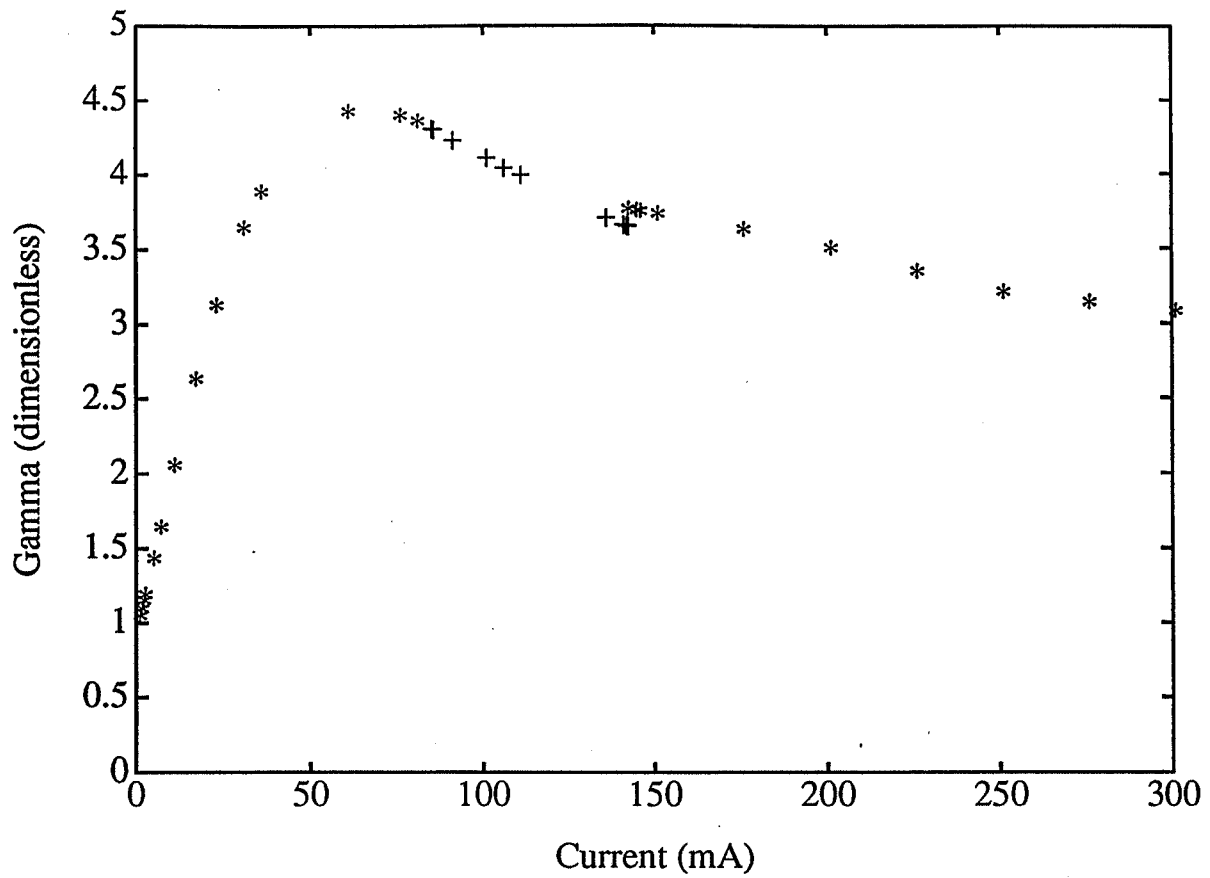
Fig. 9

Figure 14. The renormalization constant γ plotted as a function of i_d. The scales are linear, and the current range now includes the intermediate and high current regimes. In the unstable intermediate region, the average γ is plotted (+'s). The transition of γ through this unstable region is reasonably smooth.
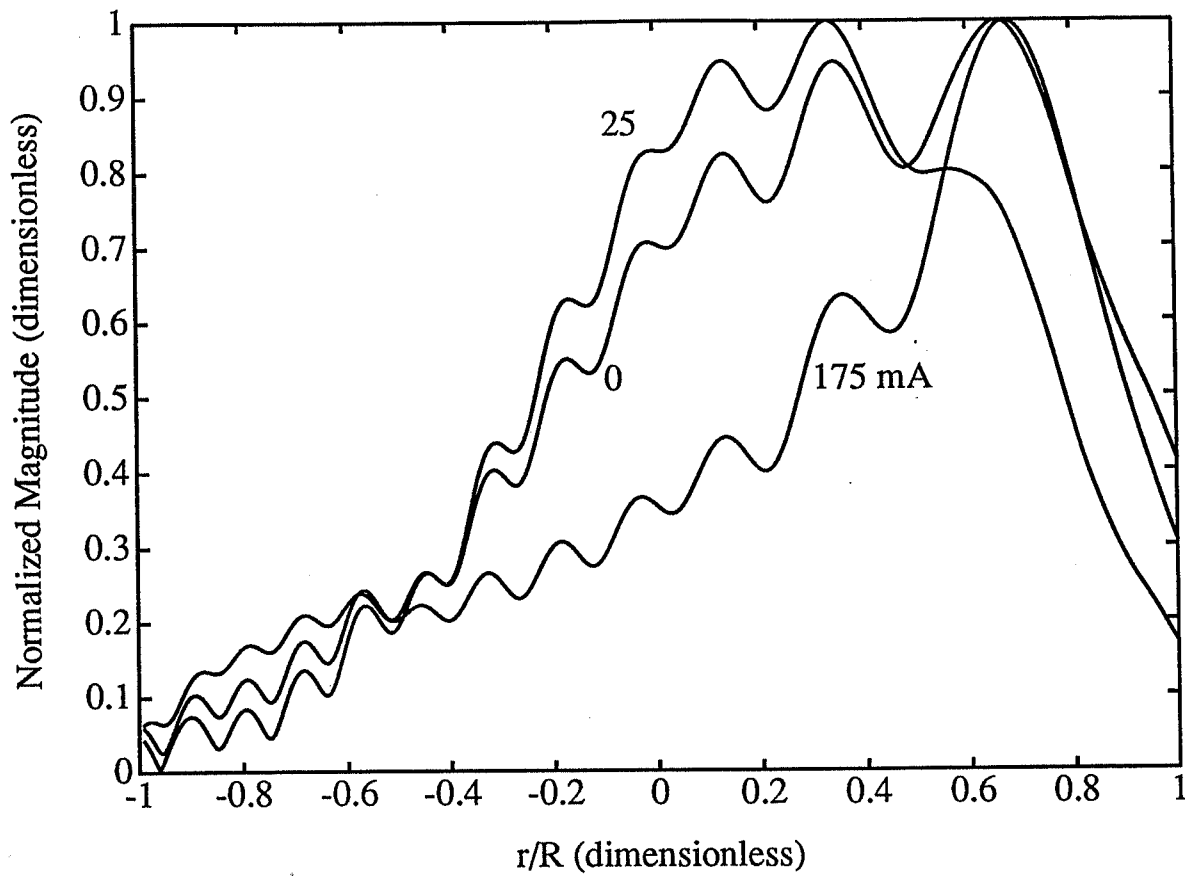
Fig. 14

Figure 10. Output field amplitudes after a single pass through an amplifier. The input was misaligned 25% relative to the axis of the amplifier. The amplifier had a radial gain dependence corresponding to currents of 0 mA, 25 mA and 175 mA. In all cases, the distortion of the beam is severe.
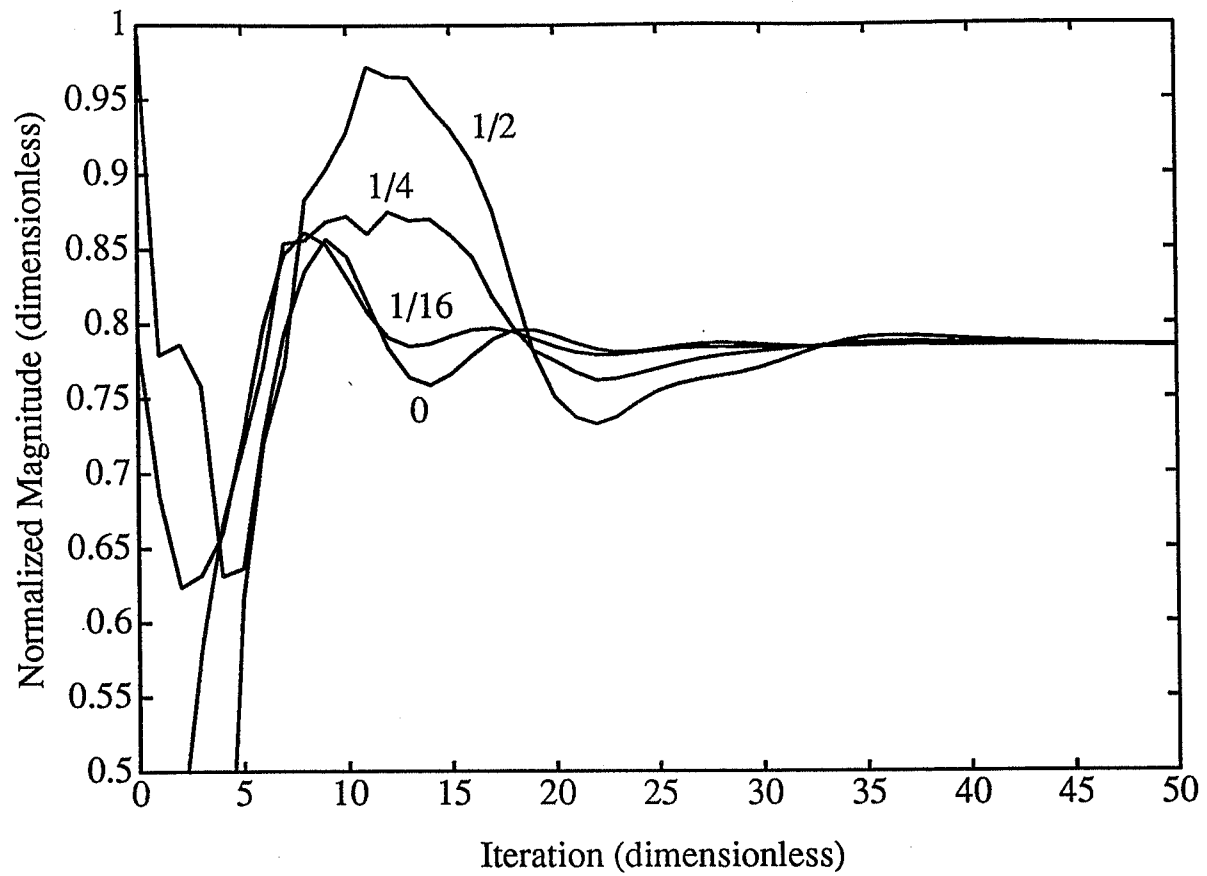
Fig. 10

Figure 11. Mode settling in a multipass amplifier with a current of $i_d = 25$ mA, for misaligned inputs of 0, 1/16, 1/4 and 1/2, relative to the radius of the cavity. All modes settle down with the same frequency and phase characteristics, but the amplitude of the swings away from steady state increases as the misalignment increases.
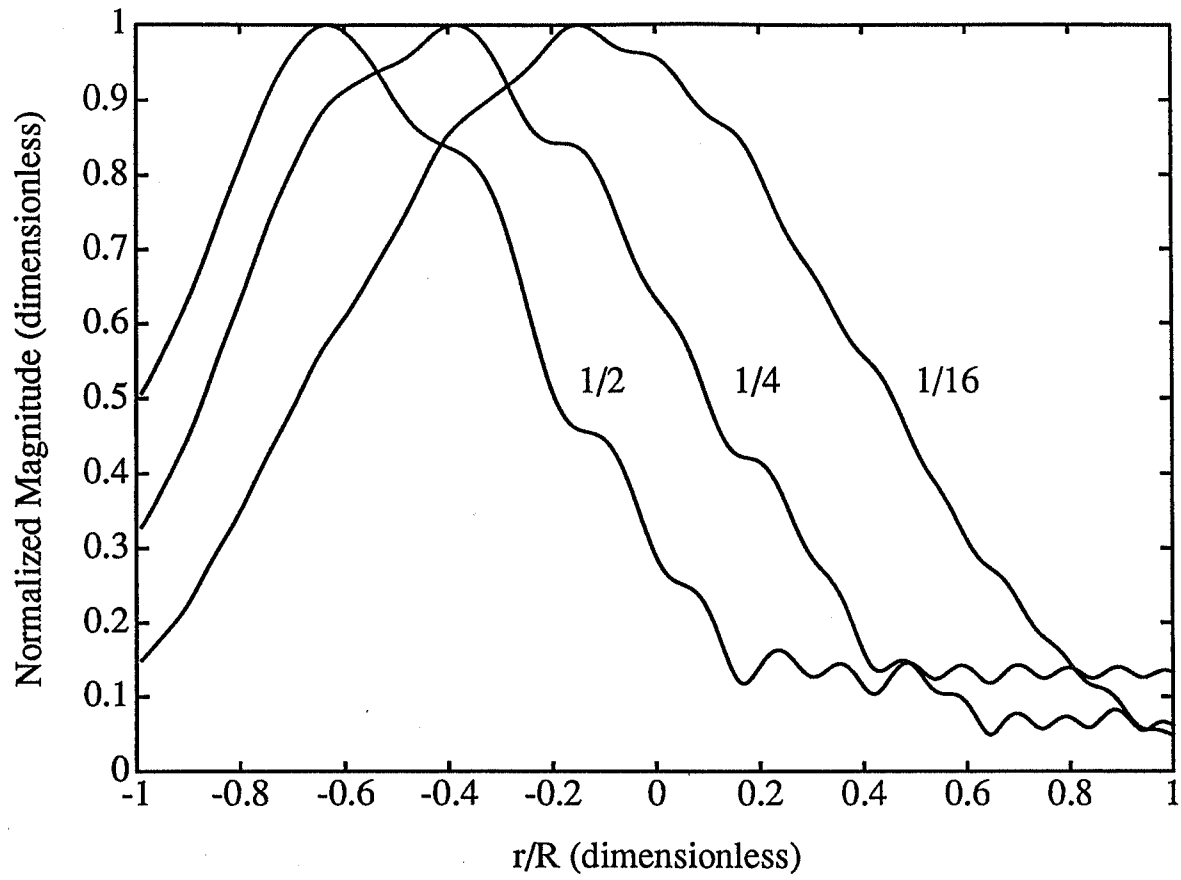
Fig. 11

Figure 12. Final mode amplitudes for a gain distribution (i_d = 25 mA) misaligned from the center line of the cavity.
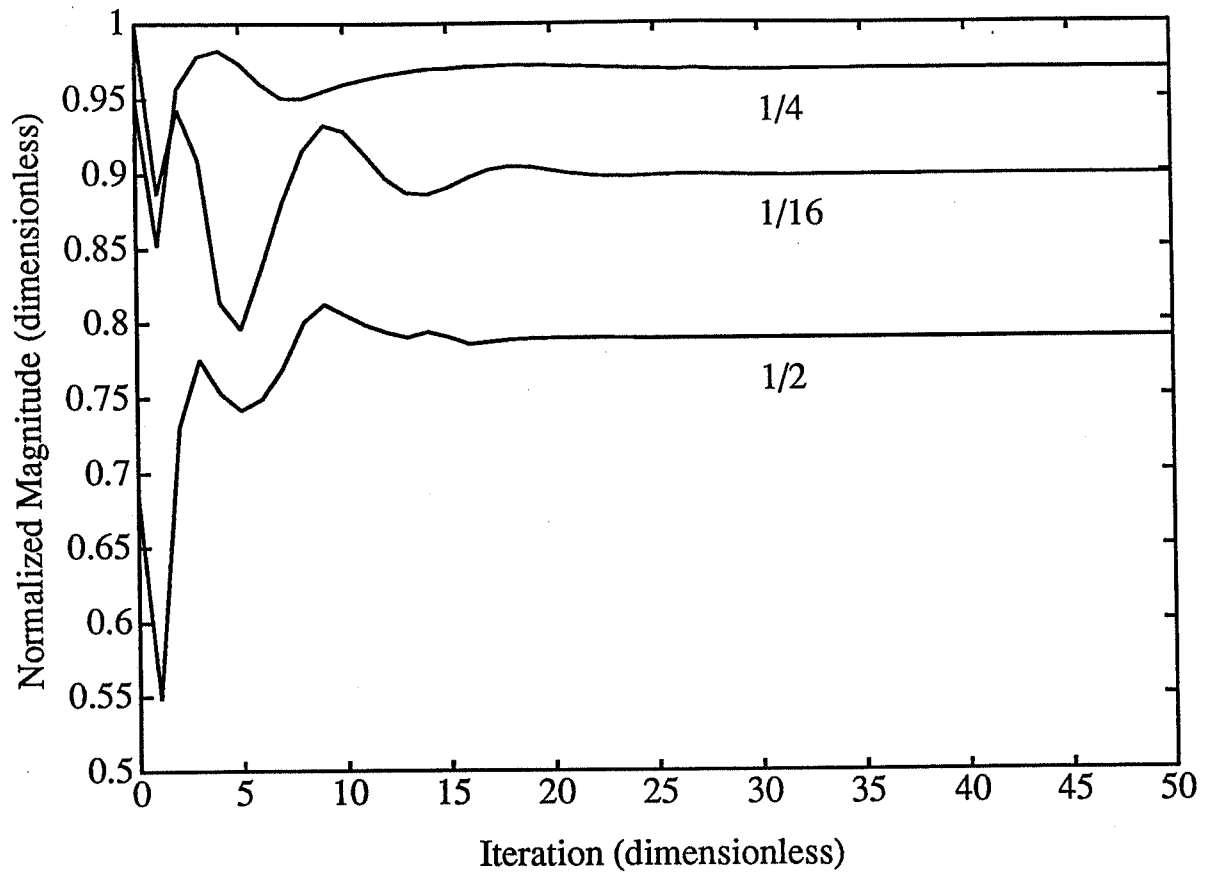
Fig. 12

Figure 13. Mode evolution for a gain distribution (i_d = 25 mA) misaligned from the center line of the cavity.

4

Fig. 13

Spherical Droplets

Mie-Debye-Lorenz Theory.

• **Spherical Harmonics**

Recent Linear Scattering Work

• **verification of Mie theory**

• **sizing of particles**

• **propagation of light through certain atmospheres**

Very high Q cavities for droplets with diameters on the order of 10 — 100 microns.

- Q's of 10^{12} — 10^{20}

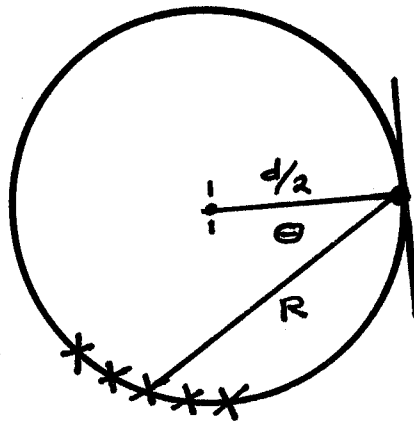- Very high concentration of energy.

Low Threshold Lasers

- Nd:YAG

- Organic Dyes

Nonlinear Scattering

- SRS

- SBS

- Sum Frequency Generation

Technique

Apodized Aperture. Fresnel Reflection.

$$\rho_s(\theta) = -\frac{\sin\left[\theta - \arcsin\left(n\sin\theta\right)\right]}{\sin\left[\theta + \arcsin\left(n\sin\theta\right)\right]}$$

$$\rho_p(\theta) = \frac{\tan\left[\theta - \arcsin\left(n\sin\theta\right)\right]}{\tan\left[\theta + \arcsin\left(n\sin\theta\right)\right]}$$

Relation to TE and TM modes.
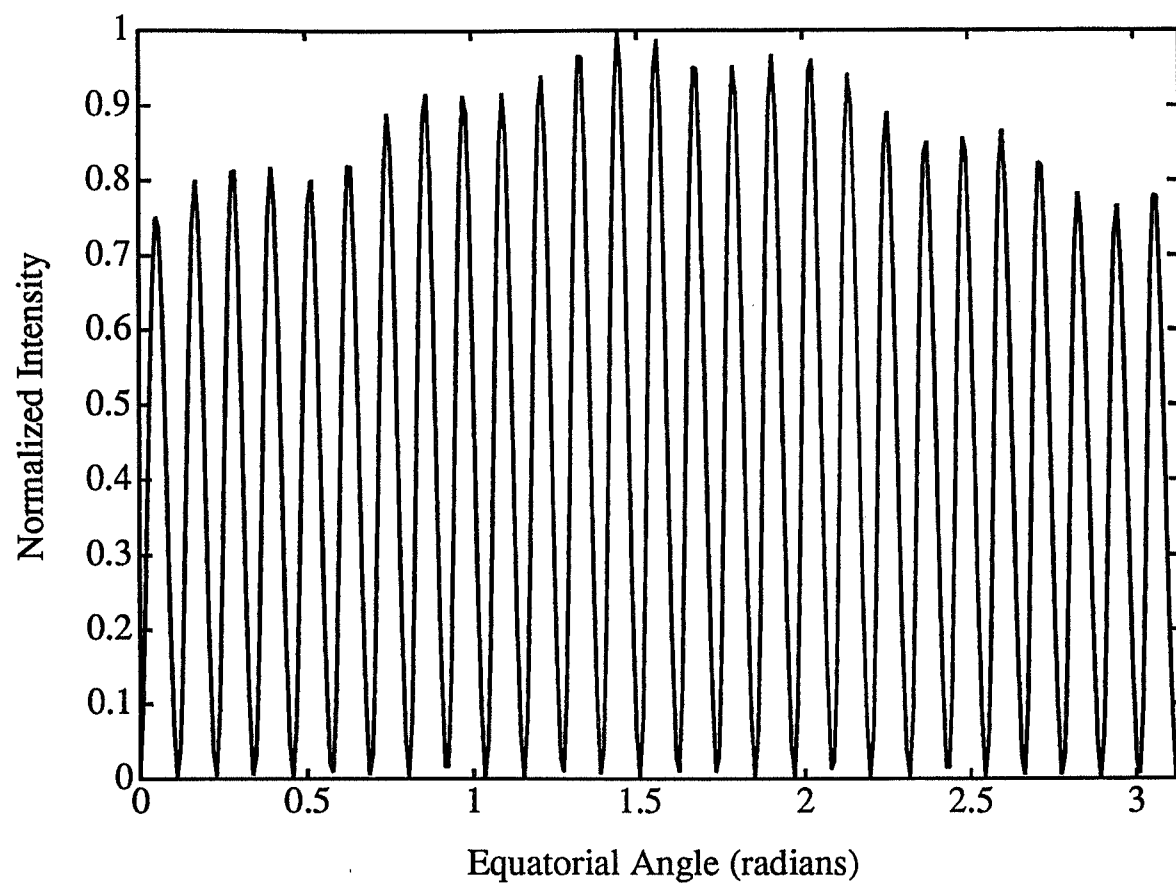
Fig. 1a

$\chi = 3\sigma\upsilon$
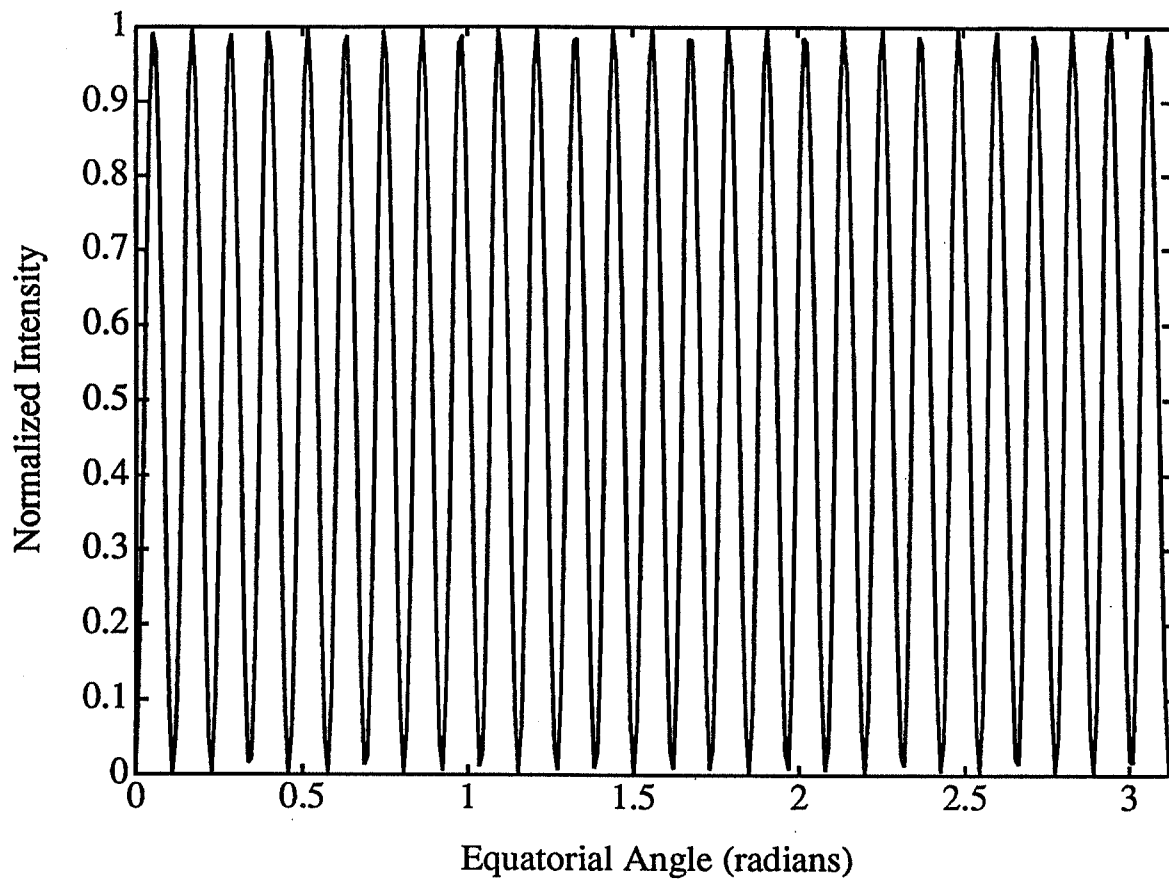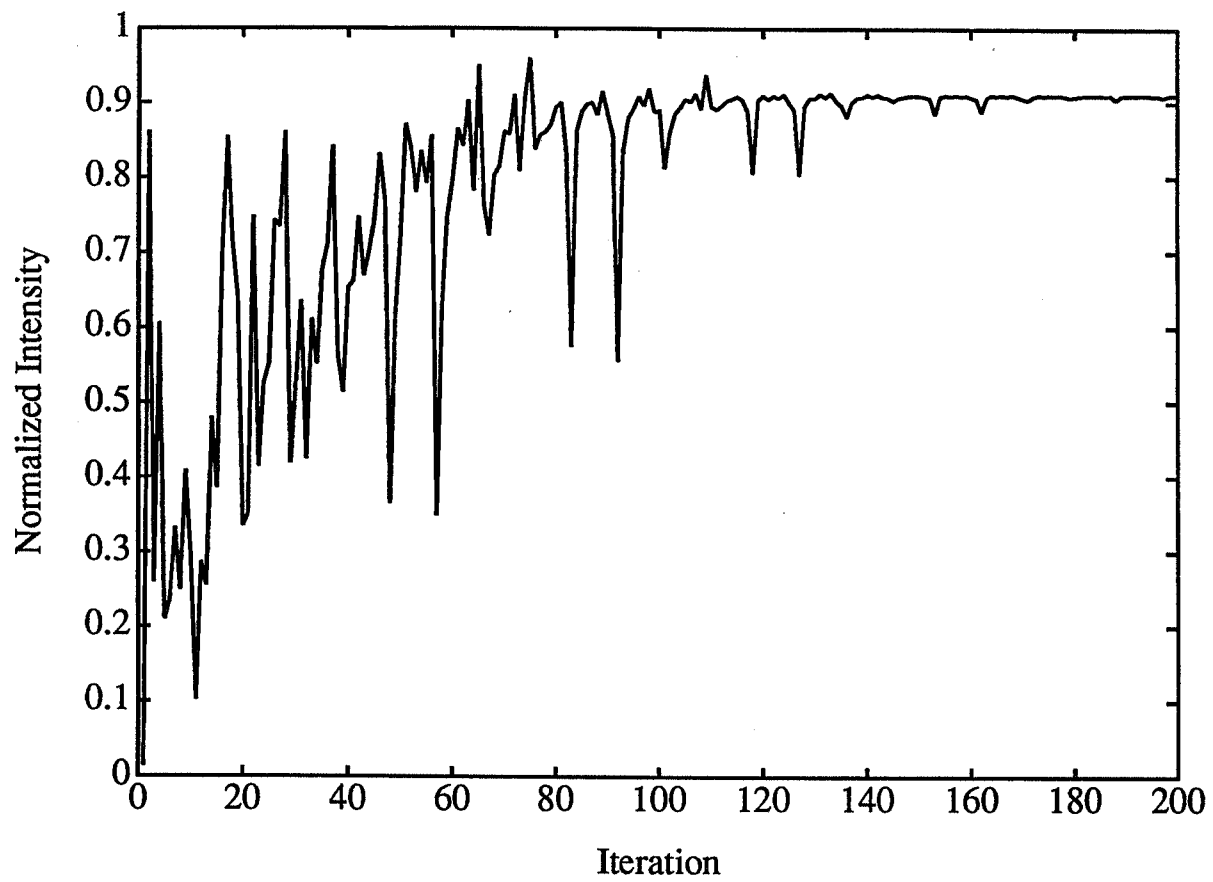
2) $\ell_{u,t_{u,t}}$
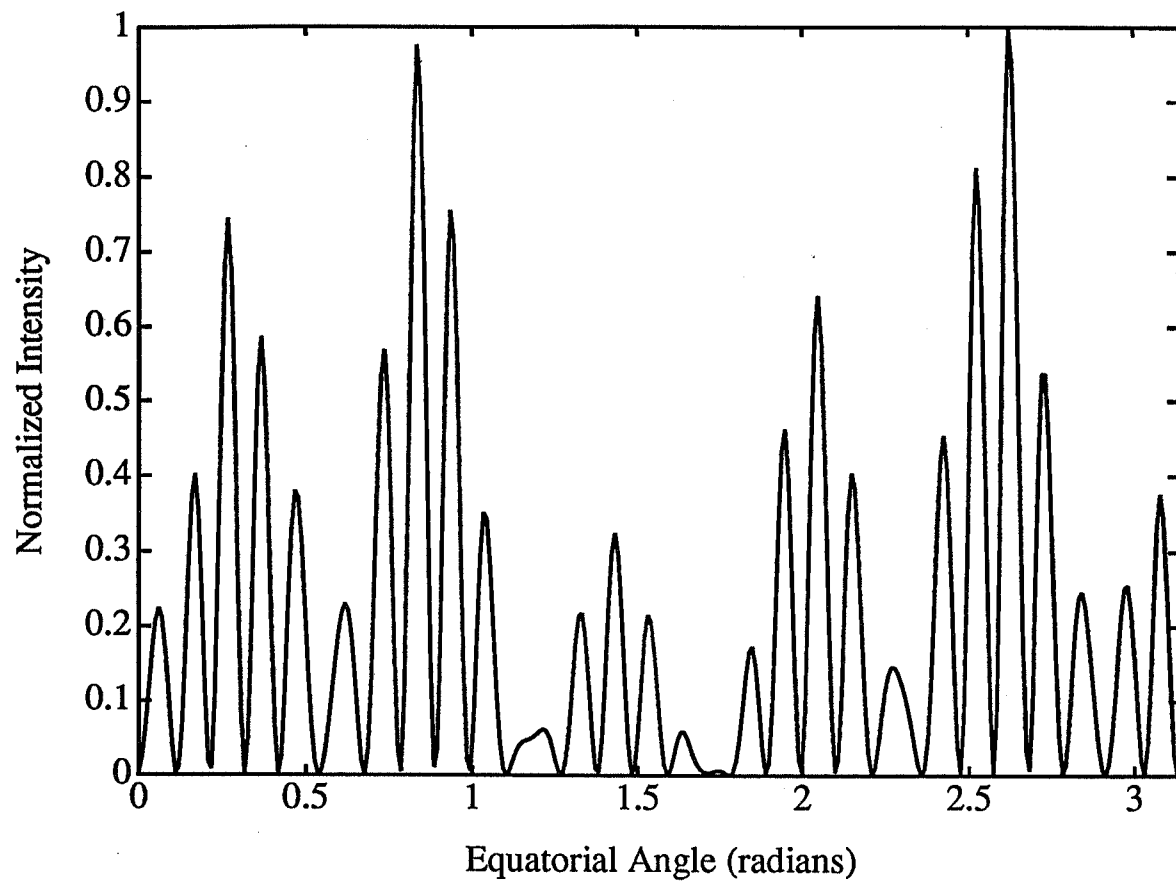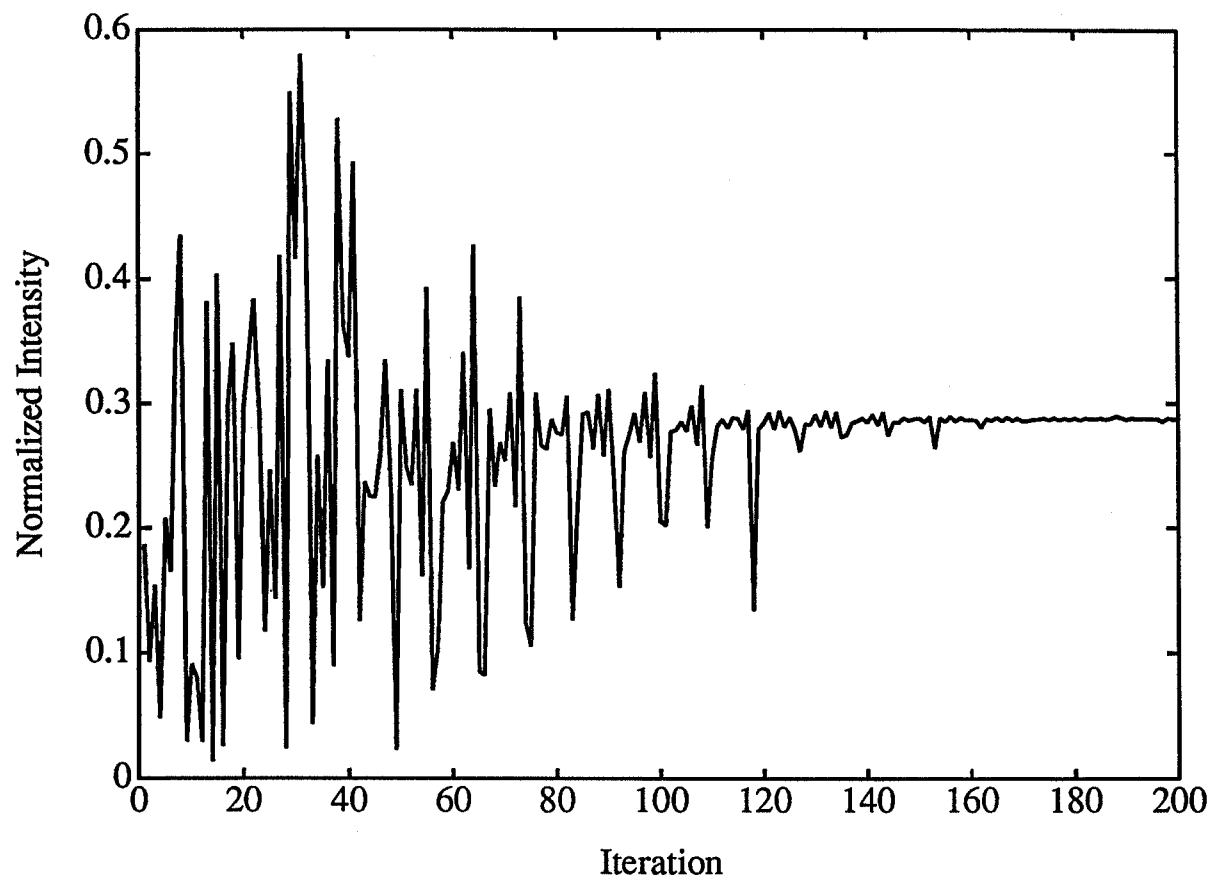
Fig. 1b

Fig 1c

Fig. 2a

Fig. 2b

Fine structures in the angular distribution of stimulated Raman scattering from single droplets

Gang Chen, William P. Acker, and Richard K. Chang

Department of Applied Physics, Yale University, New Haven, Connecticut 06520

Steven C. Hill

Department of Electrical and Computer Engineering, Clarkson University, Potsdam, New York 13676

The angular distribution of the stimulated Raman scattering (SRS) from ethanol droplets is observed to be sinusoidal with n peaks, which are consistent with the mode number n of the morphology-dependent resonances (MDR's). Two distinct values of n depend on the illumination geometry and the linewidth of the input laser radiation. Angular fine structures of the SRS can be used to identify the n of the MDR.
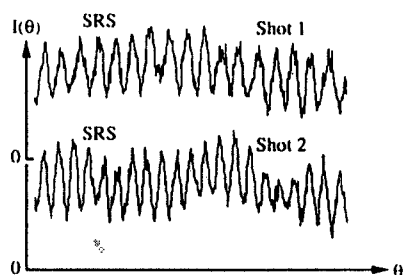
Fig. 3. For two different laser pulses (Shots 1 and 2), the $I_{\text{SRS}}(\theta)$ is different. The $I_{\text{elastic}}(\theta, \phi)$ is identical (not shown).
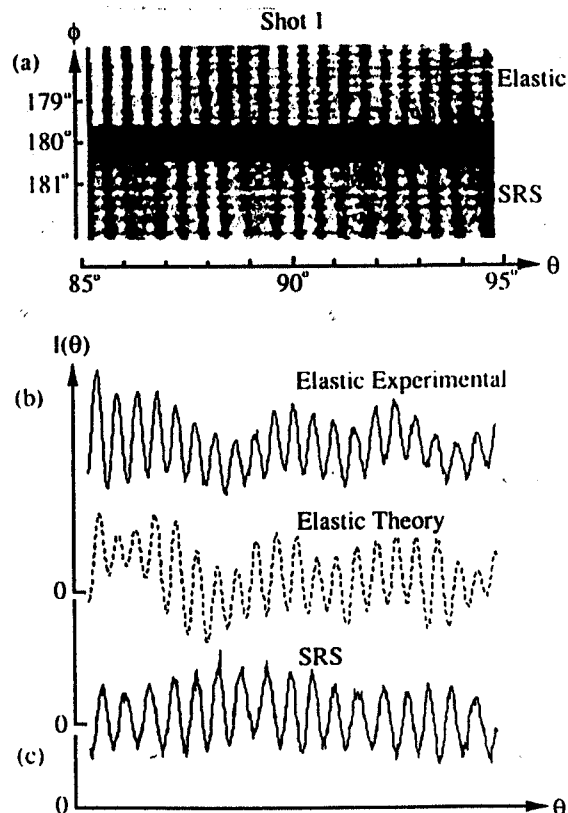

Fig. 2. (a) Gray-scale output of the CCD for one laser pulse (Shot 1) of $I_{\text{elastic}}(\theta, \phi)$ and $I_{\text{SRS}}(\theta, \phi)$. (b) Comparison of experimental and calculated $I_{\text{elastic}}(\theta)$. (c) Observed $I_{\text{SRS}}(\theta)$. The zeros of the $I(\theta)$ scale have been displaced.

Theory of nonlinear optics in dielectric spheres. III.   Partial-wave-index dependence of the gain for stimulated Brillouin scattering

C. D. Cantrell

Center for Applied Optics, University of Texas at Dallas, Richardson, Texas 75083-0688

I give analytical formulas for the gain of TE and TM electrostrictive stimulated Brillouin scattering (SBS) in a spherical microdroplet when both the laser and Brillouin frequencies coincide with single partial waves that correspond to Debye–Mie resonances.   Numerical evaluations of the analytical formula for the gain of a resonant TM mode in a water droplet show that the SBS gain peaks at the ratio η of the bulk-medium laser wavelength to the acoustic wavelength that depends on the values of the partial-wave index m for the laser and the SBS fields.   This dependence can be explained by a simple geometrical picture based on vector addition.   In the cases studied, maximum SBS gain occurs when $m_B = -m_L = \pm|l_L|$ (where l_L is the laser partial-wave order), corresponding to laser and SBS waves that counterpropagate in a tightly guided mode around a great circle of a spherical droplet.
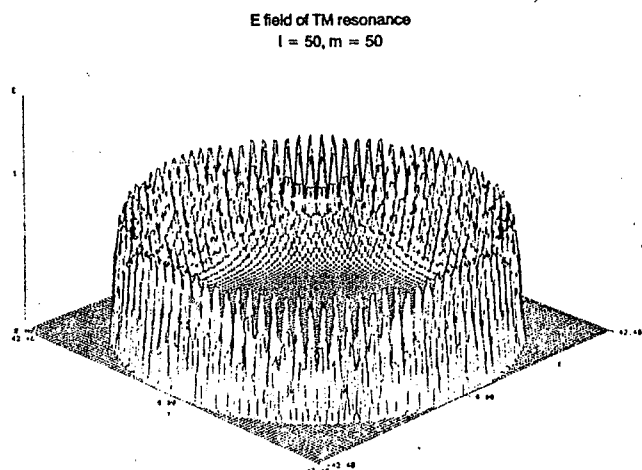

Fig. 5.   Modulus of the resonant $TM_{50,1}$ electric field as a function of r and ϕ in the equatorial plane $\theta = \pi/2$ for $|m_L| = l_L = 50$ and $k_L a = 42.4770$.
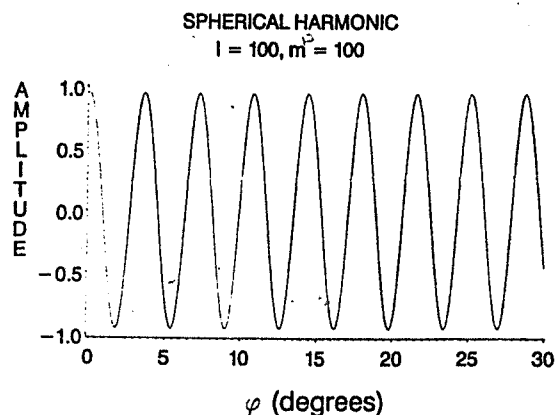

Fig. 7.   Real part of the spherical harmonic $Y_{100,100}(\theta, \phi)$ over a 30° interval in ϕ in the equatorial plane $\theta = \pi/2$.
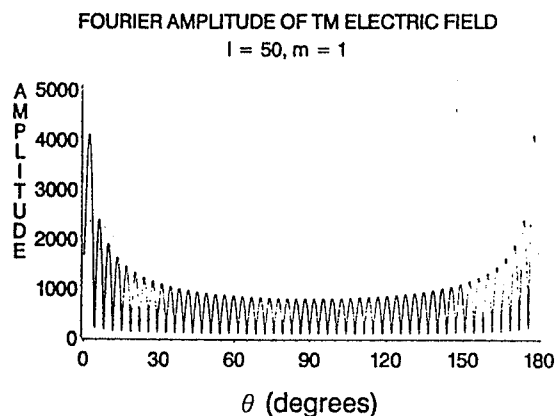

Fig. 8.   Modulus of the Fourier transform of the resonant $TM_{50,1}$ electric field as a function of θ for $|m_L| = l_L = 1$ and $k_L a = 42.4770$.

Shorter Irradiating Pulses

Mode settling time of approximately 50 psec.

• Decreased efficiency if pulsewidths are shorter than approximately 100 psec.

General Trends:

• increased droplet size decreases Fox and Li number.

• more focussed input increases mode settling time.